Targeted Dy intercalation under graphene/SiC for tuning its electronic band structure

S. Chen [1,2] Y. Han [1] M. Kolmer,[1] J. Hall,[1,2] M. Hupalo,[1] J. W. Evans,[1,2] and M. C. Tringides[1,2,*]
[1]*Ames National Laboratory-USDOE, Ames, Iowa 50011, USA*
[2]*Department of Physics and Astronomy, Iowa State University, Ames, Iowa 50011, USA*

(Received 30 June 2022; revised 16 November 2022; accepted 16 December 2022; published 9 January 2023)

Metal intercalation of graphene is a promising method to tune its electronic band structure and generate novel electronic and topological phases. The tuning depends critically on the ability to bond the intercalated atoms at predesigned, subsurface interlayer locations because the emerging band structure depends on metal location. We have studied Dy intercalation under single-layer graphene (SLG) on SiC using spot profile analysis–low-energy electron diffraction and scanning tunneling microscopy (STM). The experimental work is complemented with density-functional theory (DFT) analysis. Because different diffraction spots originate from different subsurface interlayer regions, it is possible to identify changes in the intercalation location by monitoring the spot intensity as a function of growth conditions. DFT calculations of the chemical potential as a function of intercalated Dy coverage support the variation of the stability of the intercalated phase at different intercalated locations. The preferred location is confirmed from STM studies showing the removal of the 6×6 moiré corrugation at the preferred location, observed at higher Dy coverage.

DOI: 10.1103/PhysRevB.107.045408

I. INTRODUCTION

Graphene intercalation is a robust, routine method to modify graphene's electronic properties and grow "2D" quantum materials, with targeted band structure. The interest in intercalation has been growing steadily, either of elemental quantum materials or heterostructures, as is well documented over different types of materials [1–4]. Different properties can be controlled, ranging from 2D superconductivity [5,6], heterostructure magnetization [7], spin-band polarization [8], and correlated electron physics in rare-earth layers [9]. Metal intercalation has been used both in epitaxially grown graphene on SiC (Gr/SiC) and in graphene grown on metals. Intercalation offers advantages in building heterostructures because of the intercalated metal-graphene proximity, the uniform confined spaces the intercalated metal is bonded to, and the tuning of the strength and type of metal-graphene interaction based on the atomic structure of the selected metal. The coverage and potential ordering of the intercalated phase can add a new length scale in the graphene Hamiltonian, similar to the longer length scale introduced by moiré superlattices in stacked heterostructures. The interlayer location and coverage of the intercalated metal are control parameters to realize a wealth of theoretically predicted electronic phases [1–4]. For Gr/SiC, several subsurface interlayer locations are possible, depending on the initial graphene layer [i.e., zero- or buffer-layer graphene (BL), single-layer graphene (SLG), and bilayer graphene (BLG)]. For SLG shown in Fig. 1(a), three different locations of a metal under graphene can be realized as shown schematically in Figs.1(b)–1(d). Depending on the intercalation location, the system can transform into BLG or highly doped SLG or two decoupled graphene SLG layers shifted in energy. The number of bands, band gap, effective mass, density of states, and the Fermi level can be tuned continuously, if it is possible to control reliably the intercalated metal phases. This can be done with systematic control of the growth conditions (temperature, deposited amount, annealing time). One also needs reliable characterization tools and protocols to validate the targeted atom locations and the anticipated electronic effects. Experimental work has confirmed in numerous studies how the band structure can be modified dramatically by intercalation. Decoupling from the substrate has been shown with hydrogen intercalation [10]; controlling the doping at different subsurface locations with Yb intercalation [11]; using Ga, In, and Sn intercalation to modify and protect electronic properties of the confined layers, including 2D superconductivity [6]; and controlling the size of the induced band gap in graphene by Eu intercalation at different locations [12].

Dy is a good candidate to realize topological phases because of its high atomic number *Z*. Spin-orbit coupling effects are expected to produce an effective magnetic field and the spectra to show sharp Landau levels of a 2D electron gas [13]. Split polarized bands are possible with a large band gap ~ 200 meV and a realization of the quantum Hall spin effect state [8,14] at finite temperatures. Ideal location of intercalated Dy under SLG to see topological effects is for the metal to be between BL-SiC to form BLG. A different application of intercalated Dy is based on using the hard magnetic properties of Dy; especially, if it is intercalated at the top location between graphene-BL it will demonstrate an outstanding prediction in nanomagnetism, i.e., a spring nanomagnet [15]. If a soft magnetic element like Fe is deposited on top of the intercalated Dy, the soft layer can transform to a hard, atomically thin magnetic layer of high coercivity, because of the interaction with the high Dy magnetic moment.

*mctringi@iastate.edu

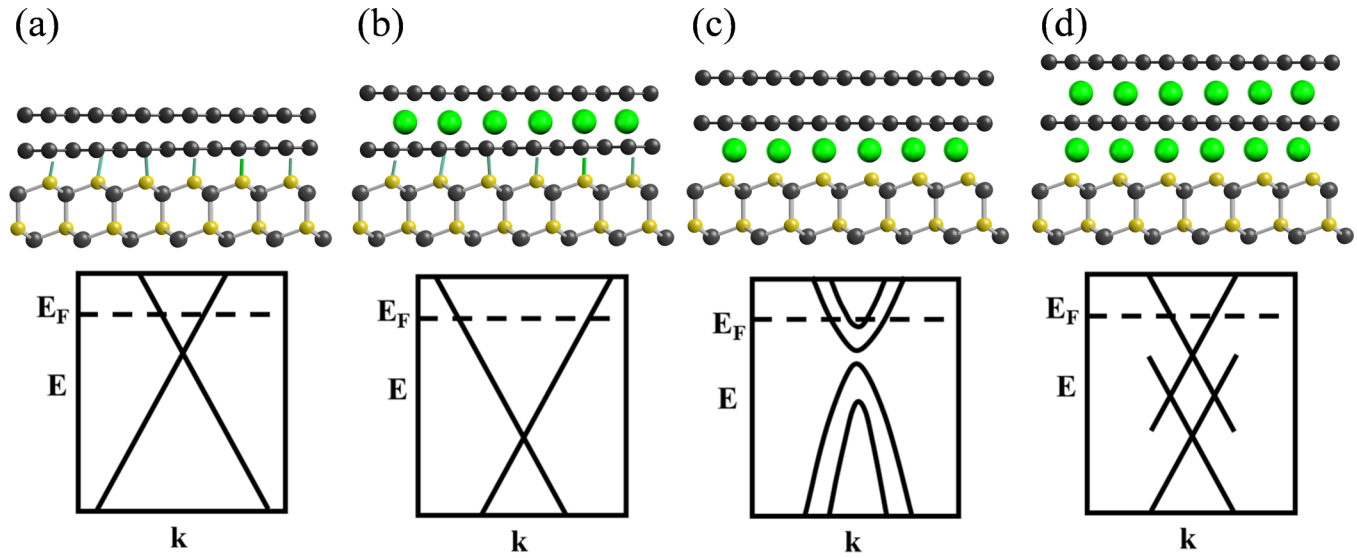

FIG. 1. Schematic showing how the intercalated metal location normal to the surface can modify dramatically the electronic band structure of SLG: (a) pristine Gr/SiC; (b) metal between graphene-BL results in higher doping level and without Dirac cone originating from the BL; (c) metal between BL-SiC results in band structure of bilayer graphene; and (d) metal at both graphene-BL and BL-SiC locations produces two decoupled linear Dirac cones doped at different levels.

Most of the intercalation work in the literature has been performed under the BL where only one location is possible. It is important to carry out experiments on thicker graphene with more available intercalation locations and therefore more possibilities to grow novel electronic phases. Only recently the same system was studied (Ca/Gr/SiC) in different experiments with the same initial phase, i.e., BLG, because the intercalated Ca was found to be a superconductor. There are three possible Ca intercalation locations: between the two top graphene layers or between graphene-ZLG or between ZLG-SiC, where ZLG is zero-layer graphene. All three locations were identified as possible intercalation locations from these recent experiments. Initially Ca was found to be between the two top graphene layers using angle-resolved photoemission spectroscopy (ARPES), low-energy electron diffraction (LEED), and scanning tunneling microscopy (STM) [16], which was later confirmed with diffraction and transport measurements [17]. A recent study using positron scattering and the dependence of the intensity vs normal component of the momentum transfer found that Ca intercalates between graphene-ZLG [18]. Another study using X-ray photoelectron spectroscopy (XPS), LEED, and STM found Ca intercalation between ZLG-SiC [19]. STM on separate graphene islands grown on SiC of different thickness found that Ca always intercalates under the top layer [20]. A more recent study has concluded that two of the three possible sites must be occupied at the same time, i.e., between graphene-BL and BL-SiC using structural techniques and ARPES [21]. This very wide range of conclusions about the intercalated metal location will lead to very different band structures and needs to be resolved, so the origin of Ca superconductivity can be identified unambiguously.

Surface diffraction is a powerful technique to study metal intercalation because one can obtain statistical information about the lateral and vertical atom distribution. Since the technique samples a submillimeter-size probed area, it can ensemble average over the mesoscale if different intercalated phases coexist. Surface x ray has been used in hydrogen intercalation studies of BL, by combining structural and spectroscopic information, to identify the atom distribution and chemical nature of the BL-SiC interface [22]. In a different study pristine Gr/SiC was studied with x-ray reflectivity to measure the density and bonding of the carbon atoms in the BL and deduce that the BL is incommensurate with the graphene layer on top [23].

In the current work using high-resolution spot profile analysis–low-energy electron diffraction (SPA-LEED), DFT, and STM, we show how changes in the location of intercalated Dy under SLG can be controlled by tuning the growth parameters (temperature, coverage, and time). A detailed protocol is followed that results in the unique identification of the intercalated metal location. Different locations under graphene give rise to distinct diffraction spots, shown schematically in Fig. 2. Changes in the spot intensities measure whether a metal has intercalated in the location generating the spot. For example, the SiC(10) spot originates from the region between BL and SiC and the 6×6 and 5/13 spots measure the area of the BL [10]. After Dy deposition the system is annealed to higher temperatures over predetermined time intervals. From the Gr(10) intensity drop we deduce that up to 1050 °C Dy occupies the graphene-BL region, but after further annealing to 1200 °C Dy bonds in the BL-SiC region. This conclusion is reached from the recovery of Gr(10) and the extinction of SiC(10) spots. Using SPA-LEED to determine the intercalated metal location from quantitative intensity measurements adds more capabilities than conventional LEED, which commonly relies on visual inspection of the diffraction pattern. Ideally it would be desirable to be able to carry *I-V* measurements with LEED to determine the exact coordinates of all type of atoms present on the surface [24]. Unfortunately, the complexity of the $6\sqrt{3} \times 6\sqrt{3}$ unit cell is too high. Just for pristine SLG it involves the top four layers of the graphitized substrate with a

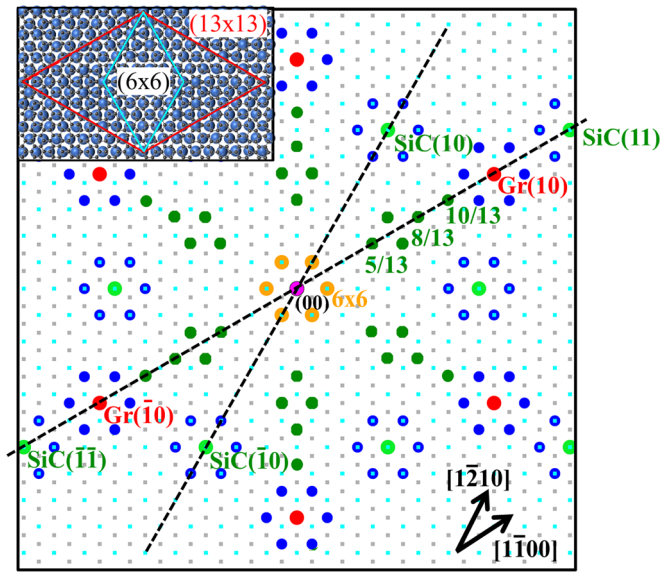

FIG. 2. Schematic of the SLG diffraction pattern with graphene fundamental spots in red and SiC fundamental spots in light green. The higher-order spots originate from the real-space supercell shown at the inset of the top left corner. This supercell is $13a_G \times 13a_G$ along the graphene direction which is made of 3 $6a_{SiC} \times 6a_{SiC}$ along the SiC direction. Higher-order spots discussed in the text are also marked. The two scan directions in Figs. 3 and 4 are shown with dashed lines.

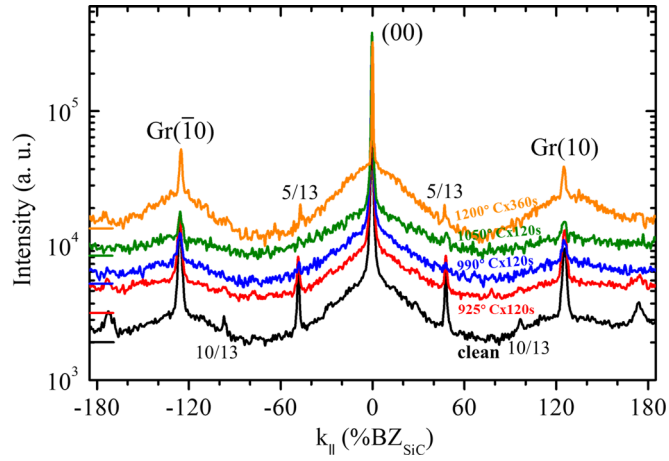

FIG. 3. Dy intercalation of SLG graphene with 2 ML Dy. SPA-LEED profiles along [1$\bar{1}$00], with bottom profile showing pristine graphene; the next three profiles are obtained after annealing for 2 min at 925 °C, 990 °C, 1050 °C, and the top one for 6 min to 1200 °C. The intensities are shifted with the bars indicating the same count level. At 1050 °C Gr(10) becomes almost extinct (green), indicating that Dy occupies the graphene-BL location.

total of 558 atoms; the complexity of the unit cell will further increase after metal intercalation and the different possibilities for the metal to intercalate. At this stage the determination of the structure of such large unit cell is prohibitively costly and has not been completed yet [24].

DFT calculations verify that the most stable location for Dy with increasing coverage switches from the graphene-BL to the BL-SiC region, and that the corresponding interlayer spacing increases considerably to accommodate the intercalated metal. The conclusion is confirmed with local STM images that show that the 6×6 superstructure is completely removed as the Dy bonds between BL-SiC (after stepwise annealing and increasing Dy coverage). The 6×6 moiré superstructure with period ∼1.84 nm is observed for pristine Gr/SiC as a coincidence lattice at the BL-SiC interface.

Such intercalation protocol can be applied with any quantitative diffraction probe and can settle incompatible conclusions about the intercalation location. More importantly, it provides a robust methodology to grow on-demand, targeted electronic phases. The metal atoms can be directed to specific interlayer locations, as required by the theory predicting the novel electronic phases.

II. EXPERIMENT

Experiments were performed in UHV with pressure $\sim 5 \times 10^{-11}$ Torr. The growth of high-quality graphene on 4-H SiC(0001) was carried out at high temperatures to desorb Si while C diffuses and forms large uniform domains [25]. By flashing within 1200 °C–1400 °C for short 15 s intervals, graphene of different thickness can form, starting with the BL and finishing with the trilayer [26]. Spot profiles along different directions are used to deduce the initial graphene thickness. The current surface was prepared at 1300 °C and is more than 90% SLG as deduced from quantitative analysis of the 00 and Gr(10) spots [and their corresponding bell-shaped-components (BSCs)]. These paradoxically broad diffraction features were shown to be markers of high-quality graphene [27]. Dy was deposited with a flux rate of ∼1/60 ML/min at room temperature for a total of ∼2 ML. Annealing was carried out using e-beam heating with temperature calibration based on the well-known Pb/Si(111) phase transitions [28].

The instrumental resolution is less than ∼ 0.3% of the Brillouin zone (BZ) (or the coherence length is larger than ∼300 nm.) Since the spots are measured simultaneously using the difference of spot intensity from their clean surface values, the assignment of intercalated metal location is complete and self-consistent. The difference from the clean spot intensity is a measure of the intercalated amount. $E = 194$ eV was used to probe with higher sensitivity deeper in the surface. STM provides mainly information about the 6×6 superstructure of ∼1.84-nm period. It is used to deduce that the most stable metal intercalation site is BL-SiC, since the 6×6 periodicity is globally removed after annealing to the higher temperature.

III. RESULTS

A. Diffraction

Figure 3 shows results for Dy intercalation of SLG graphene after annealing 2 ML Dy deposited at room temperature. For rare-earth metals higher temperatures are needed to overcome the high kinetic barriers of intercalation [29]. The profiles are along [1$\bar{1}$00] (the Gr(10) direction), with the bottom profile corresponding to pristine graphene, the next three after annealing for 2 minutes at 925 °C, 990 °C, and 1050 °C, and the top one after annealing for 6 min to 1200 °C. The intensities are shifted for clarity with the bars to the left

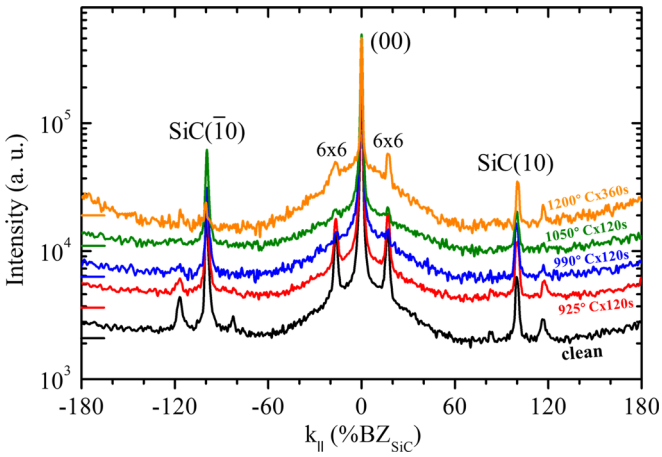

FIG. 4. Dy intercalation of SLG graphene with 2 ML Dy. SPA-LEED profiles are along [1$\bar{2}$10] (for the same annealing sequence as in Fig. 1.) Up to 1050 °C, the SiC(10) spot is still strong. At 1200 °C the profiles (orange) show that 00, SiC(10), its 6 × 6, decrease dramatically from their clean values. These changes show that Dy, which was initially between graphene-BL, has moved between BL-SiC.

indicating the same count level. The 00 and Gr(10) show also the BSCs around each spot, which are affected less with annealing. As seen at 1050 ° C the Gr(10) becomes almost extinct (green), indicating that Dy atoms occupy mainly the graphene-BL location. Figure 4 shows the corresponding profiles along [1$\bar{2}$10] (the SiC direction) for the same annealing sequence. Up to 1050 °C, the SiC(10) is still strong. But, at 1200 °C the profiles (orange) show that some spots increase substantially compared to the spots at 1050 °C [Gr(10), the two BSCs around 00 and Gr(10)], while others [00, SiC(10), its 6 × 6] decrease dramatically from their clean surface values. These changes imply that Dy which was initially between graphene-BL has moved between BL-SiC, so the Gr(10) intensity increases while the SiC(10) intensity decreases as Dy atoms bond on top of SiC.

Spot profile fitting was used for quantitative analysis, deducing the variation of the integrated areas, the full width at half maxima (FWHM), and the peak intensities with annealing temperature. These metrics have quantitative information about the location and coverage of the intercalated metal. For the fits, Lorentzian functions with an exponent of 3/2 (LRZ-3/2) were used. Some of the fits are shown in Supplemental Material, Figs. S1–S4 [30]. Table I shows the extracted integrated areas for the spots along [1$\bar{1}$00] and Table II shows the analogous parameters along the [1$\bar{2}$10] direction. These quantitative fits follow the spot dependence with annealing as described qualitatively in the previous paragraph. The results are plotted in Fig. 5(a) showing the spots which have relatively large values: the narrow 00 component along [1$\bar{1}$00] (black), the BSC of 00 along [1$\bar{1}$00] (deep green), and the BSC of Gr(10) (blue). The narrow 00 component drops continuously while the two BSCs have only small variation. Figure 5(b) shows intensities of spots with relatively low values: [the SiC(10), its 6 × 6, the 6 × 6 around 00, Gr(10), and 5/13 spots]. The Gr(10) (purple) and the 6 × 6 around 00 (red) recover partially towards their pristine values. The other three spots SiC(10) (orange), its 6 × 6 (black), and the 5/13 (cyan) become practically extinct at 1200 °C. The most spectacular variation is the one from SiC(10) and its 6 × 6, which drop by an order of magnitude; considering also the Gr(10) increase, this confirms the Dy transfers to BL-SiC.

Figures 6(a)–6(d) shows schematically the different steps in the experiment: starting from pristine SLG [Fig. 6(a)], after deposition of Dy on top [Fig. 6(b)], after annealing to 1050 °C with Dy between graphene-BL [Fig. 6(c)], and after annealing to 1200 °C with Dy between BL-SiC [Fig. 6(d)]. These results show that intercalation is mostly a kinetic process with controllable locations for the intercalated metal, depending on growth conditions. The different Dy intercalated phases can be used to tune the intercalated Dy band structure.

B. Theoretical analysis

Calculations have been performed to determine Dy adsorption energetics over different types of steps present on SLG separating graphene and BL regions [29]. Such steps are likely places for Dy deposited on top to move below graphene. The stability of the intercalated phases and location of the intercalated metal were studied for different Dy coverages $\theta = 1/16$ ML, 1/4 ML, and 1 ML. But, no discussion was made in connection to experiments as the ones described in this work, especially to identify the trend of the intercalated metal location as a function of Dy coverage. Three bonding sites were tested: on top, within graphene-BL, and within BL-SiC. Results are shown in Fig. 7 with both the calculated interlayer spacing and the corresponding chemical potentials listed at the two subsurface locations. The spacings of pristine graphene are 0.23 nm for BL-SiC and 0.33 nm for graphene-BL.

TABLE I. Integrated areas for the listed spots as a function of annealing temperature along the [1$\bar{1}$00] direction. Lorentzian functions with exponent 3/2 (LRZ-3/2) were used for the fits.

Annealing step	E/eV	Constant background	Specular		Gr(1̄0)	
			Narrow	Broad	Narrow	Broad
Pristine	194	1900	2.6×10^5	2.3×10^5	3.2×10^4	5.6×10^4
925 °C × 120 s	194	2600	2.2×10^5	1.7×10^5	2.3×10^4	3.5×10^4
990 °C × 120 s	194	1900	1.7×10^5	1.8×10^5	6.3×10^3	4.3×10^4
1050 °C × 120 s	194	1900	9.9×10^4	1.5×10^5	4.0×10^3	3.0×10^4
1200 °C × 360 s	194	1500	3.8×10^4	2.2×10^5	9.1×10^3	7.8×10^4

TABLE II. Integrated areas for the listed spots as a function of annealing temperature along the [1$\bar{2}$10] direction. Lorentzian functions with exponent 3/2 (LRZ-3/2) were used for the fits.

Annealing step	E/eV	Constant background	Specular		Left 6 × 6 of (00)	SiC ($\bar{1}$0)	Left 6 × 6 of SiC($\bar{1}$0)
			Narrow	Broad			
Pristine	194	1900	3.9×10^5	2.3×10^5	2.9×10^4	4.8×10^4	1.5×10^4
925 °C × 120 s	194	2600	3.2×10^5	1.7×10^5	2.0×10^4	3.2×10^4	6.1×10^3
990 °C × 120 s	194	1900	2.4×10^5	1.9×10^5		2.3×10^4	
1050 °C × 120 s	194	1900	1.4×10^5	1.5×10^5	1.8×10^3	2.5×10^4	
1200 °C × 360 s	194	1500	6.3×10^4	2.2×10^5	9.7×10^3	3.2×10^3	2.3×10^3

For $\theta = 1/16$ ML the most stable site is between graphene-BL with a chemical potential $\mu = -4.61$ eV; the corresponding spacing increases to 0.42 nm [29]. For $\theta = 1/4$ ML the two locations become comparable ($\mu = -5.48$ eV for graphene-BL and $\mu = -4.96$ eV for BL-SiC) and again the intercalation location increases to 0.44 nm while the location without Dy keeps its pristine value. This result is consistent with the earlier conclusions that the BL-SiC is preferred at 1200 °C, since the experiments were carried out at high Dy coverage. The calculations are based on the widely used $(2\sqrt{3} \times 2\sqrt{3})R30^\circ$ unit cell (in the theoretical literature [29]) to model the BL $6\sqrt{3} \times 6\sqrt{3}$ unit cell present in Gr/SiC; for $\theta = 1/4$ ML 4 Dy atoms are bonded within the unit cell. For even higher coverage $\theta = 1$ ML (16 Dy atoms bonded within the $2\sqrt{3} \times 2\sqrt{3}$ unit cell, i.e., much larger compression) the BL-SiC becomes the most stable location ($\mu = -4.79$ eV), but because of the large compression Dy forms a bilayer and the interlayer spacing more than doubles to 0.74 nm. Although such high coverage will not be attained for the intercalated Dy, the DFT results suggest a monotonic decrease of the chemical potential with coverage. The BL-SiC location becomes the most stable site and its interlayer spacing continuously increases with θ. (Ge intercalated in Gr/SiC has two different intercalated phases, n-doped with 1 ML and p-doped with 2 ML forming a p-n junction [31]). The n-doped phase with 2 ML coverage is a likely realization of the phase predicted for $\theta = 1$ ML in Fig. 7 with the double-intercalated layer and the very large increase of the interlayer spacing. The interlayer spacing increase at the metal location is also seen in other DFT studies of metal intercalation in Gr/SiC. Both the experimental and theoretical results listed demonstrate that besides intercalation controlled mainly by kinetics, the competition between elastic and electronic energies plays a role to define the most stable location, within the confined spaces in the interior as analyzed in Ref. [32]. This competition accounts for the larger interlayer spacing with increasing metal coverage.

C. STM

The change of intercalation location observed in the diffraction experiments and in the calculations at finite coverage is confirmed in STM experiments of SLG intercalation shown in Fig. 8. A similar Dy deposition experiment was performed as before with the initial surface morphology shown in Fig. S5(a) over the mesoscale. A line scan in Fig. S5(b) shows that the step heights separating adjacent terraces are multiples of 0.25 nm: the step height of SiC. This implies that the grown graphene layer is homogeneous draping SiC steps of differing heights. The initial Dy morphology after deposition is seen in Fig. S5(c). Figure 8(a) shows clean graphene with both the graphene lattice and the typical 6 × 6 corrugation of ∼1.84-nm period defect-free. As discussed, changes in the intercalated phase are induced from variations in the controlled parameters (coverage, time, temperature, etc.). The previous theoretical prediction of Fig. 7 about intercalated phase stability can be tested with STM. The STM provides local images and there might be a distribution of intercalated phases present on the surface after annealing, especially of coexisting phases

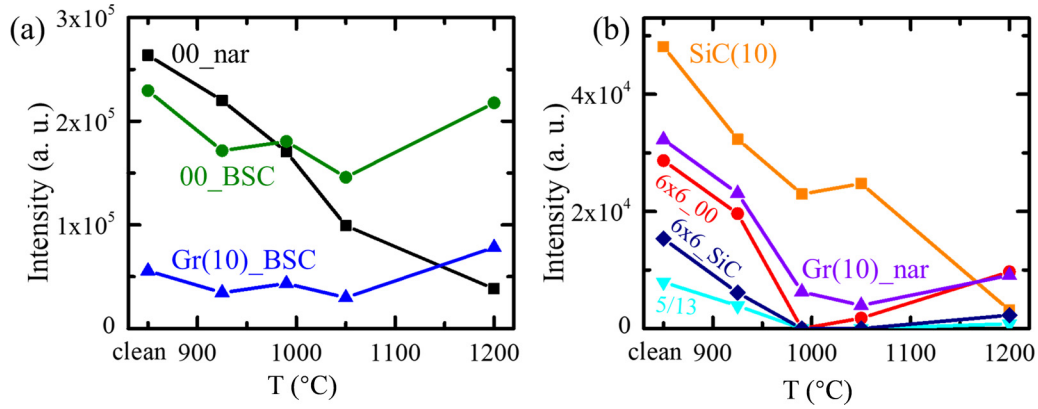

FIG. 5. Variation of integrated spot area with annealing temperature. (a) Spots with relatively large values: the narrow 00 component (black), the BSC of 00 (deep green) and the BSC of Gr(10) (blue). (b) Spots with relatively low values: [SiC(10), its 6 × 6, 6 × 6 around 00, Gr(10), and 5/13 spots]. SiC(10) (orange), its 6 × 6 (black), and the 5/13 (cyan) become practically extinct at 1200 °C.

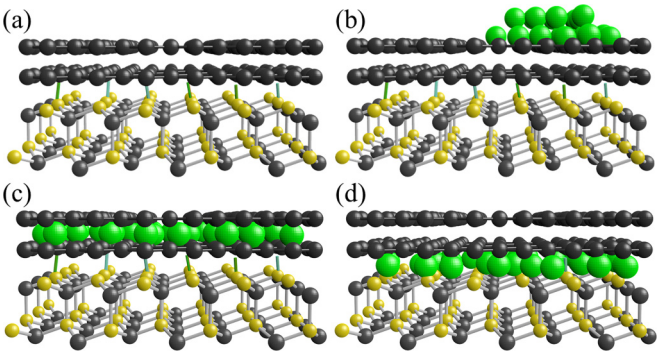

FIG. 6. (a)–(d) Schematic of the different steps in the experiment: (a) pristine SLG; (b) after deposition of Dy; (c) after annealing to 1050 °C with Dy between graphene-BL; and (d) after annealing to 1200 °C with Dy between BL-SiC.

with similar energetic stability. But, the coverage which is uniformly deposited across the whole surface is a better parameter to control the uniformity of the intercalation outcome. Figure 8(b) shows a typical image of the surface after smaller amount 0.8 ML Dy deposition and stepwise annealing for 30 min from 450 °C to 900 °C. No Dy islands are on top indicating that Dy has moved below SLG. One-dimensional scan for pristine surface is seen in Fig. 8(d), with both the graphene lattice of lattice constant 0.245 nm and the 6 × 6 periodicity ∼ 1.8 nm clearly visible. One-dimensional (1D) scan for the phase of Fig. 8(b) is seen in Fig. 8(e). Although the ∼1.8-nm periodicity is present, indicating that there are still 6 × 6 domains, there is still large modulation of the amplitude of the 1D scan and a small fraction of linear segments without the 6 × 6 periodicity. The presence of 6 × 6 confirms that the intercalated Dy is not between BL-SiC, as also deduced previously from the strong 6 × 6 spots in the diffraction profiles colored green in Figs. 1 and 2. A small fraction of Dy atoms within BL-SiC could be responsible for the lower amplitude between the regions with strong 6 × 6 intensity. Figure 8(c) shows the outcome covering globally the surface after further deposition of 1.5 ML Dy, followed again by gradual heating over the same temperature range 450 °C to 900 °C. No sign of the 6 × 6 remains, demonstrating that all the intercalated Dy has now moved in the BL-SiC region. This is also confirmed in the 1D scan of Fig. 8(f). The graphene lattice is clearly resolved on top of this disordered intercalated Dy phase [seen at the inset of Fig. 8(c)], which further supports that the phase is below graphene and homogeneous. The stepwise deposition and stepwise annealing of Dy is needed so the already intercalated Dy moves in the interior away from the entry portals and additional Dy entering the portal can complete a more uniform intercalated phase within BL-SiC as shown in Fig. 8(c).

In addition, Figs. 9(a)–9(c) show the autocorrelation of the previous images, Figs. 8(a)–8(c), which provide further support about the changes in the intercalated surface for different growth conditions. Figs. 9(d)–9(f) show 1D scans marked with green dotted lines in the autocorrelation images, Figs. 9(a)–9(c). In Fig. 9(d) the very regular 1.8-nm periodicities of the 6 × 6 and 0.245 nm of pristine graphene are seen. In Fig. 9(e) periodicities close to the 6 × 6 periodicity (1.7, 1.8, and 1.9 nm) of the 0.8 ML Dy phase are seen but of reduced amplitude. As discussed earlier a small fraction of disorder is generated by Dy atoms starting to occupy the BL-SiC location. In Fig. 9(f) after the additional 1.5 ML Dy deposition and annealing to 900 °C, the 1.8-nm periodicity is absent, indicating full intercalation at the higher coverage. The regularity of the 6 × 6 phase is a sign whether the buffer layer-SiC interlayer location is occupied by intercalated Dy.

IV. DISCUSSION

The previous results have shown how the intercalation location can change with annealing or increasing coverage and how the new location can be identified unambiguously with complementary diffraction, STM, and DFT techniques. Such characterization is relevant to more recent intercalation studies, since there is growing interest to use a wider range of deposited metals and/or initial graphene phases. As discussed in the Introduction, Ca intercalation in BLG was found to be a 2D superconductor. This is the only system for which many different studies have been performed for the same metal and the same initial graphene surface [16–21]. Unfortunately, all three intercalation locations for BLG were identified as possible sites, and even joint occupation of the two deeper locations has been deduced in the latest publication [21], which raises the number of intercalation possibilities even more. This and similar conflicting identifications should be resolved quickly and robustly; otherwise, different band structures and inconsistent 2D physical mechanisms for the superconductivity will be deduced from experiments. Part of this disagreement is related to using video LEED only qualitatively from the visual inspection of the spots, which also depends on contrast settings of the detector camera. Using the variation of all the spots and measuring their intensities quantitatively as in the current work can remove the ambiguity. The Ca studies have also demonstrated the increase of interlayer spacing at the Ca intercalation location analogous to the Dy results; in Ref. [19] the spacing of the BL-graphene was found to be 0.42 nm and in Ref. [18] the spacing between BL-SiC was found to be 0.47 nm.

Besides the Ca controversy, the growing intercalation literature shows other systems where different locations or intercalated phases have been identified, which further points to the value of quantitative diffraction. When ZLG was used as the initial graphene phase, there is only one location for the metal to bond, so it is not possible to have inconsistent assignments in metal location. However, when thicker graphene was used and the same metal was deposited different intercalation locations were identified. We briefly list several systems in the literature which show resolving conflicting identifications is a more general challenge. Although ZLG-SiC is the most stable location expected from the majority of experiments and DFT calculations, this is not always the extracted intercalation location.

When SLG was used as the initial surface and Au was intercalated at 850 °C [33], it was found that the intercalation location was between graphene-ZLG but not ZLG-SiC as found in Refs. [34,35]. In the Au intercalation experiments under SLG two coexisting intercalated phases were identified: a phase with intercalated clusters and a phase with moiré

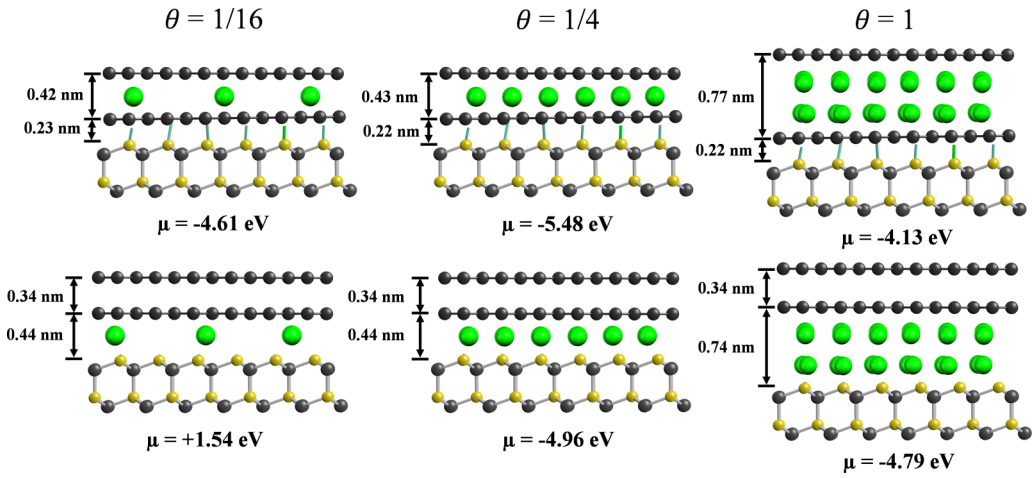

FIG. 7. Theoretical calculations of the most stable intercalation location for different Dy coverages $\theta = 1/16$ ML, 1/4 ML, and 1 ML. Interlayer spacing and chemical potentials are listed at the two subsurface locations BL-SiC and graphene-BL.

$(2\sqrt{3} \times 2\sqrt{3})R30^\circ$ pattern (located between graphene and BL). Au intercalation of the BL (despite only one possible intercalation location) has shown two differently doped Au phases: a *p*-doped (1/3 ML) phase and an *n*-doped (1ML) phase. Similar experiments with Co intercalated at 400 °C have reached the same conclusion about graphene-ZLG as the bonding location [36] but not ZLG-SiC as in Refs. [37,38]. Tb intercalates at 600 °C in SLG but both graphene-ZLG and ZLG-SiC locations were found to be occupied jointly [39]; Rb intercalated at −190 °C in BLG (with three possible singly occupied locations as in the Ca experiments) bonds between first and second graphene layers as expected for alkali metal intercalation of graphite [40]; Eu intercalates at 300 °C under SLG at both locations depending on temperature, i.e.,

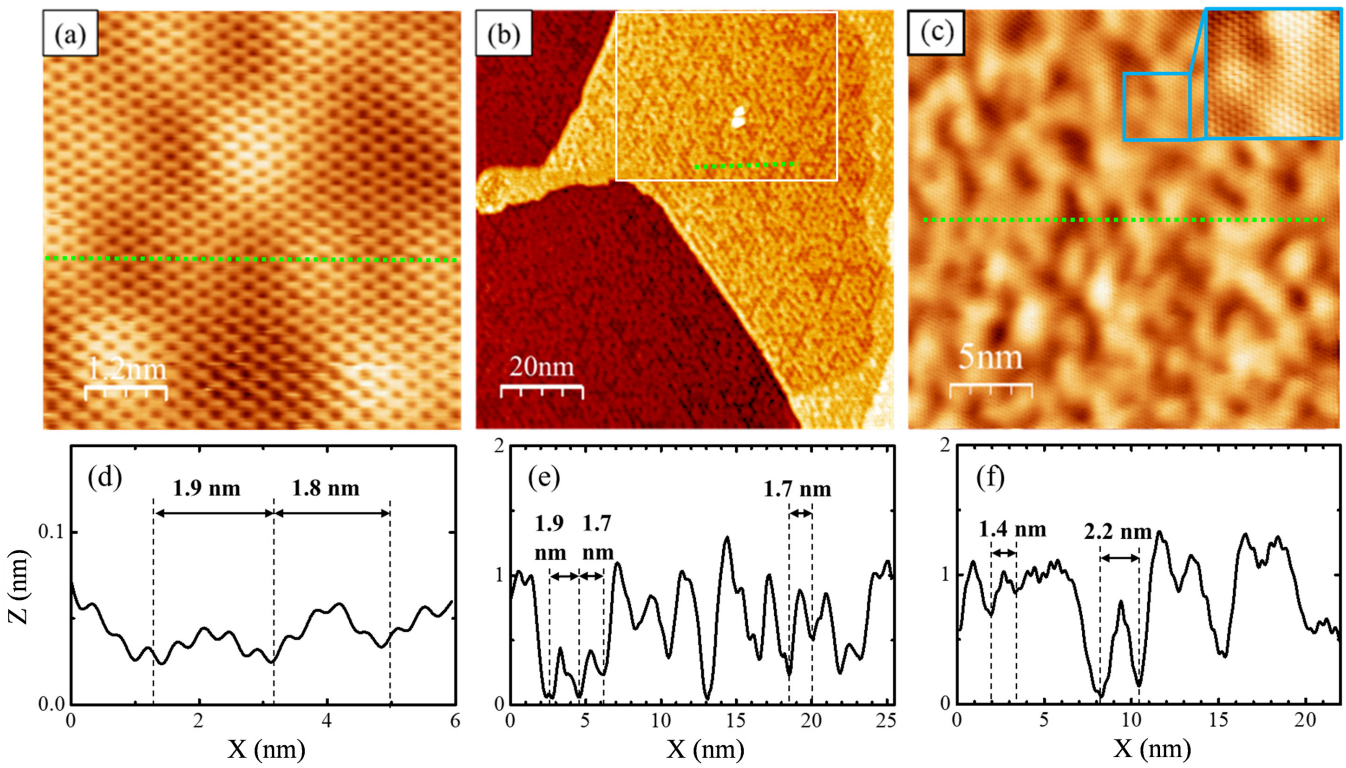

FIG. 8. (a) Clean SLG with the typical 6 × 6 moiré of nominal ∼1.84-nm period. (b) Image after 0.8 ML Dy is annealed stepwise for 30 min from 450 °C to 900 °C. Although the 6 × 6 is present, a small fraction of the area does not have the periodicity. The 6 × 6 confirms that the intercalated Dy is between graphene-BL. (c) Image after further deposition of 1.5 ML Dy followed by annealing from 450 °C to 900 °C. No 6 × 6 is present indicating that Dy is in the BL-SiC region. The graphene lattice is resolved on top of the intercalated disordered phase (see inset, top right corner). Image parameters: (a) 0.39 V, 0.46 nA; (b) 1.5 V, 1.0 nA; (c) −0.4 V, 2.4 nA; (d) one-dimensional scans of (a) showing both 1.8-nm periodicity of the 6 × 6 and 0.245-nm graphene periodicity. (e) One-dimensional scans of (b) showing mostly the 6 × 6 periodicity but also a small fraction of the area without it. (f) One-dimensional scans of (c) showing no 6 × 6 periodicty.

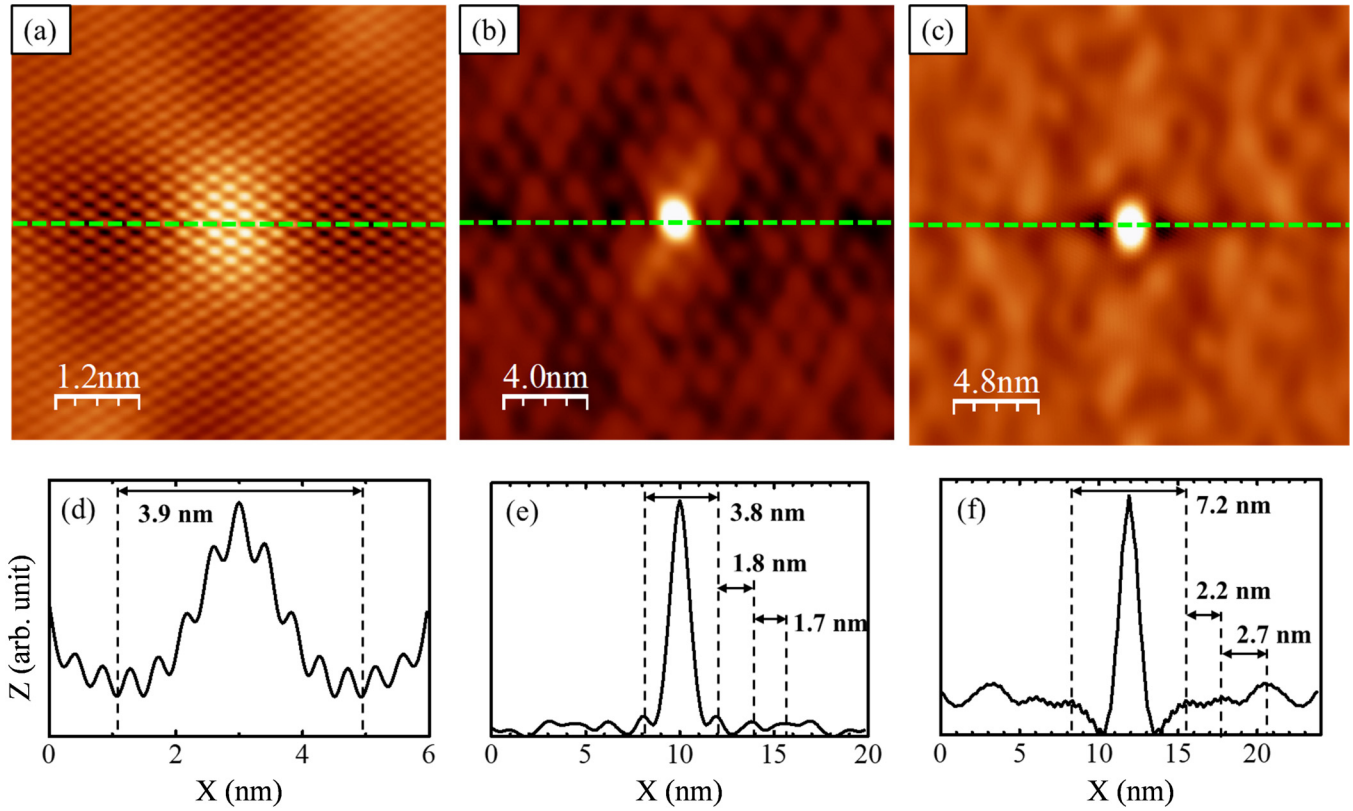

FIG. 9. Autocorrelation of the previous images [Fig. 8(a)–8(c)] of (a) pristine graphene (b) of the intercalated phase after 0.8 ML Dy deposition and annealing to 900 °C with the 6 × 6 periodicity still present (c) of the disordered Dy intercalated phase after the additional 1.5 ML Dy deposition and annealed to 900 °C with the 6 × 6 periodicity absent. (d) One-dimensional scan of (a) showing both periods of the 6 × 6 and graphene. (e) One-dimensional scan of (b) showing the ∼ 1.8-nm period of the 6 × 6 is still present but of reduced amplitude. (f) One-dimensional scan of (c) showing that no 6 × 6 periodicity remains.

between graphene-ZLG at 120 °C and between ZLG-SiC at 300 °C [12].

In the current Dy intercalation experiments we have varied the growth conditions from room temperature to higher temperature, so it is possible to capture all the intercalated phases that form, including metastable ones. Predominantly intercalation is determined by kinetics, i.e., by the energetic barriers that control the transfer of the deposited atoms to subsurface locations. These barriers include adatom diffusion on top to reach the entry portals and surface diffusion within the inner spaces that control adatom spreading and aggregation to form subsurface structures. It is more common in the literature to deposit an initial large amount of the metal of interest, followed by one-step annealing to sufficiently high temperature, searching for the absence of the 6 × 6 spots that indicates occupation of the BL-SiC location. This is usually complemented by XPS that gives information about the transfer of atoms below, but with limited sensitivity to the intercalation location, especially for thicker graphene. Such one-step annealing might bypass phases that are kinetically easier to form and are favored at lower temperatures.

In the literature Gd intercalation has been studied under the BL [9]. It is remarkable that the growth conditions to intercalate Gd are analogous to the ones used in the current Dy experiments, although the initial surface in the two experiments is different, i.e., BL vs SLG. After Gd deposition, annealing to 800 °C–1200 °C results in uniform disordered intercalated layer without the 6 × 6 periodicity. Clearly surface diffusion in the two systems is comparable, since relative high temperatures are needed to induce structural changes in the distribution of the intercalated atoms. On the other hand, comparison with other rare-earth metals shows that for these metals, the temperatures at which atoms transfer below are much lower: Yb (250 °C) [11], Tb (600 °C) [39], and Eu (120 °C–300 °C) [12], most likely because the interaction between these metals and C atoms is much weaker than the interaction of Dy and Gd with C atoms.

In Ref. [9], Gd doping of the BL was sufficiently high to reach the Van Hove singularity at the *M* point, resulting in an intercalated phase of strong homogeneity and stability. Flat bands developed which were confirmed in theoretical studies. Novel ordered electronic states driven by electronic correlations and high density of states at the *M* point are expected to form in such systems. A different study [41] using high-resolution scanning tunneling microscopy and spectroscopy (STM/STS) maps of Gd intercalation under bilayer graphene (with three intercalation locations possible) has also shown similar high doping for the lower two bands (with Gd occupying the BL-SiC and graphene-BL locations). The dI/dV maps provide both the phase morphology (from topographic images) and the local density of states (from STS spectra). A uniform high coverage ∼2 ML Gd phase intercalated at 1200 °C under BLG was grown. This Gd phase has analogous growth procedure and is morphologically similar to

the Dy phase shown in Fig. 8(c). Since unusual high-level doping was seen for Gd intercalation in the two experiments under BL [9] and BLG [41], one should expect that Dy intercalated under SLG should also have high doping levels reaching the *M* point. Correlated electron physics and flat bands should be expected for Dy. Using SLG as the initial substrate, only two bands will be present and heavily doped. The interaction between the two linear bands at the points they cross can lead to nonlinearities in the energy dispersion, potentially can open large energy gaps, and change the electron effective mass. Analogous electronic effects related to the crossing of linear bands were shown in several earlier studies of SLG [39,42], but the linearity of the band dispersion was attributed to the presence of a fraction of *AA* regions within the normal *AB* stacked regions, which partially results in sample electronic inhomogeneity. Since by controlling both the Dy coverage and annealing temperature, the dopant location can be tuned gradually between graphene-BL to between BL-SiC, this eventually will change the massless linear Dirac cones to massive parabolic bilayer bands.

Examining the spot intensities in Tables I and II and Fig. 5 in more detail, we can follow how changes of other spots can clarify further the intercalation process. The narrow component of the 00 spot over the full annealing range decreases by a factor of 5 from its clean value, while as noted, the BSC increases by a factor of 1.5. The 00 spot has contribution from any type of disorder at all graphitized layers, probed at the relative high electron energy of 194 eV, while the BSC to be discussed further below originates from the top layer as implied by electron confinement and is not sensitive to deeper defects.

Concerning the Gr(10) spot and its BSC, they have lower integrated areas than the corresponding ones of the 00 spot by a factor of ∼10, while the corresponding FWHM of the Gr(10) is larger by factor of 3 than the FWHM of the 00 spot. (FWHM values are listed for the four profiles shown in the Supplemental Material.) This can be related to the presence of different types of orientational graphene domains because graphene has threefold symmetry. These domains are separated by antiphase domain boundaries and can be abundant on the surface as imaged by low-energy electron microscopy (LEEM) with their lateral sizes smaller than 100 nm [45]. Because the Gr(10) wave vector has nonzero parallel momentum transfer it is sensitive to the finiteness of the domains and the intervening domain boundaries. The 00 spot has no parallel momentum transfer and is not sensitive to lateral domain boundaries. It can explain why it is stronger and with smaller FWHM than the Gr(10) spot. The complexity of the BL-SiC interface, with the structure of the $6\sqrt{3} \times 6\sqrt{3}$ large supercell still not determined, is also seen from the way different 6×6 spots behave with annealing. As seen from Table II, the 6×6 spots surrounding the SiC spot become extinct with annealing at 1200 °C and the transfer of Dy between BL-SiC, while the 6×6 spots surrounding the 00 spot still have finite intensity. This shows that other factors control how these 6×6 spots are generated, which results in nonequivalent spots depending on the adjacent fundamental spot, i.e., whether the 00 or the SiC(10).

The behavior of the different diffraction spots with annealing can also shed more light on the origin of the bell-shaped-component (BSC). There is need for routine diagnostic tools, especially to confirm the thickness uniformity of 2D materials. We have demonstrated that the BSC is a very strong broad background in surface electron diffraction from graphene [27]. The FWHM can be unusually large, ∼ 50% BZ, but paradoxically it is a very useful marker of high-quality graphene. This diffuse intensity follows the Bragg component as a function of electron energy, which is the opposite of what is expected in normal interference scattering when the diffuse intensity should be anticorrelated to the Bragg peak. The BSC has been present in numerous graphene studies over the last ∼25 yr but totally ignored by the community [27]. At least three different systems [Gr/SiC, Gr/Ir(111), and h-BN] [27,43] were studied quantitatively with similar large FWHM ∼ 50% BZ of the BSC. In addition, in all three systems the BSC-integrated intensity is at least one order of magnitude larger than the Bragg component-integrated intensity, which points to a strong and universal mechanism generating the BSC. A plausible origin of the BSC is electron confinement within a uniform graphene layer (or in other 2D materials) that causes a spread in their normal wave-vector component [44]. This spread is transferred to the parallel component of the diffracted electrons via strong interaction between graphene electrons and incident beam electrons.

The Dy annealing experiments at 1200 °C of Figs. 3 and 4 show that after Dy is transferred in BL-SiC, although the Gr(10) spot increases it does not fully recover to its initial value for the clean surface; on the other hand the BSC returns back to its pristine value. This suggests that the Gr(10) spot is sensitive both to the top graphene layer and the BL (which almost has the same crystalline structure as graphene but different band structure). Dy below BL after annealing to 1200 °C can lower the Gr(10) intensity. On the other hand the BSC most likely is only sensitive to the graphene layer (as implied by the confinement model and because the pure BL layer shows no BSC). This explains why the BSC recovers to its pristine value after 1200 °C, since its intensity is not affected by Dy atoms intercalated under the BL. It most likely implies that the BSC is a stronger marker of graphene thickness uniformity than the Gr(10) spot.

As mentioned earlier, the intercalated Dy between graphene-BL will be a candidate to realize a spring magnet, i.e., a structure with a layered hard magnet in contact with layered soft magnet, both structures grown as ultrathin films. The proposal has been in the literature for some time and discussed in Ref. [15]. Such concept requires growing on the nanoscale with the proximity of the two layers critical to maximize the exchange interaction, which causes the high coercive field of the hard magnet to increase the coercivity of the soft magnet. Growing Fe film on top of intercalated Dy under graphene fulfills the proximity condition and adds chemical passivation to the Dy layer, because it is covered by graphene on top. In addition, the single-layer thickness of the soft magnetic layer avoids one major challenge, i.e., magnetization twisting for thickness comparable to the domain-wall width of the soft layer. Magnetic heterostructures based on graphene intercalation have been already implemented in the literature demonstrating strong interaction between the orbitals of the intercalated metal and the orbitals of the metal on top. A Co-Gr-Fe heterostructure was grown on Gr/Ir(111) with Co below and Fe on top [7].

x-ray magnetic circular dichroism (XMCD) shows that the Fe film has opposite magnetization from the intercalated Co; thus, the heterostructure can be used as antiferromagnetic filter, ideal for spintronics. In a different study an intercalated magnetic layer in contact with topological insulator thin film has generated magnetic topological phases in the composite system [46].

Besides magnetic effects it was shown that the interaction between the subsurface metal layer and the deposited metal on top is sufficiently strong to affect other atomistic processes, such as nucleation and surface diffusion on top. Studies were performed on mixed substrate of intercalated and nonintercalated regions. Eu island nucleation was preferred on nonintercalated than intercalated regions of Gr/Ir(111) [47]. In Ref. [48] Dy adatom random-walk diffusion was changed to biased random-walk diffusion transferring deposited atoms to the intercalated areas under Gr/SiC. Using ARPES and theoretical modeling was another way to account for changes of the band structure after K deposition at low temperature on BL [49]. For this nonintercalated system a higher fraction of K is adsorbed on top than at the interior interfaces, which generates charge asymmetry and opens a large energy gap. But, no change of metal location with potentially tunable electronic phases was shown, as in the current intercalation studies.

V. CONCLUSIONS

It is important to control metal intercalation of Gr/SiC, especially if the initial surface is thicker than BL because different intercalation locations are possible. The emerging band structure depends on the subsurface metal location, so control of the intercalation location provides a way to generate a wealth of electronic phases. Using Dy intercalation under SLG as a prototype, we show from quantitative analysis of the diffraction spots with annealing that the metal intercalation location can be controlled from graphene-BL to BL-SiC. DFT calculations show that as the Dy coverage increases, the preferred intercalation site becomes BL-SiC, with a corresponding large increase in the interlayer spacing. The preference for BL-SiC as the intercalated site is further supported by STM studies that show the 6×6 becomes extinct with gradual annealing and increasing Dy coverage, confirming that Dy prefers the BL-SiC location. This intercalation protocol can be applied in other experimental systems to control metal intercalation in a similar way and show how a class of 2D electronic materials can be generated via predictive and targeted intercalation.

ACKNOWLEDGMENTS

This work was supported by the U.S. Department of Energy (DOE), Office of Science, Basic Energy Sciences, Materials Science and Engineering Division. J.W.E. was supported by the USDOE Chemical Sciences, Geosciences, and Biosciences Division. The research was performed at Ames Laboratory, which is operated for the U.S. DOE by Iowa State University under Contract No. DE-AC02-07CH11358.

[1] L. Daukiya, M. N. Nair, M. Cranney, F. Vonau, S. Hajjar-Garreau, D. Aubel, and L. Simon, Functionalization of 2d materials by intercalation, Prog. Surf. Sci. **94**, 1 (2019).

[2] J. Wan, S. D. Lacey, J. Dai, W. Bao, M. S. Fuhrer, and L. Hu, Tuning two-dimensional nanomaterials by intercalation: Materials, properties and applications, Chem. Soc. Rev. **45**, 6742 (2016).

[3] N. Briggs, Z. M. Gebeyehu, A. Vera, T. Zhao, K. Wang, A. De La Fuente Duran, B. Bersch, T. Bowen, K. L. Knappenberger, and J. A. Robinson, Epitaxial graphene/silicon carbide intercalation: A minireview on graphene modulation and unique 2d materials, Nanoscale **11**, 15440 (2019).

[4] X. Zhao, P. Song, C. Wang, A. C. Riis-Jensen, W. Fu, Y. Deng, D. Wan, L. Kang, S. Ning, J. Dan, T. Venkatesan, Z. Liu, W. Zhou, K. S. Thygesen, X. Luo, S. J. Pennycook, and K. P. Loh, Engineering covalently bonded 2d layered materials by self-intercalation, Nature (London) **581**, 171 (2020).

[5] E. Mazaleyrat, S. Vlaic, A. Artaud, L. Magaud, T. Vincent, A. C. Gómez-Herrero, S. Lisi, P. Singh, N. Bendiab, V. Guisset, P. David, S. Pons, D. Roditchev, C. Chapelier, and J. Coraux, How to induce superconductivity in epitaxial graphene via remote proximity effect through an intercalated gold layer, 2D Mater. **8**, 015002 (2020).

[6] N. Briggs, B. Bersch, Y. Wang, J. Jiang, R. J. Koch, N. Nayir, K. Wang, M. Kolmer, W. Ko, A. De La Fuente Duran, S. Subramanian, C. Dong, J. Shallenberger, M. Fu, Q. Zou, Y. W. Chuang, Z. Gai, A. P. Li, A. Bostwick, C. Jozwiak, C. Z. Chang, E. Rotenberg, J. Zhu, A. C. T. van Duin, V. Crespi, and J. A. Robinson, Atomically thin half-van der Waals metals enabled by confinement heteroepitaxy, Nat. Mater. **19**, 637 (2020).

[7] P. Gargiani, R. Cuadrado, H. B. Vasili, M. Pruneda, and M. Valvidares, Graphene-based synthetic antiferromagnets and ferrimagnets, Nat. Commun. **8**, 699 (2017).

[8] I. I. Klimovskikh, M. M. Otrokov, V. Y. Voroshnin, D. Sostina, L. Petaccia, G. Di Santo, S. Thakur, E. V. Chulkov, and A. M. Shikin, Spin-orbit coupling induced gap in graphene on Pt(111) with intercalated Pb monolayer, ACS Nano **11**, 368 (2017).

[9] S. Link, S. Forti, A. Stöhr, K. Küster, M. Rösner, D. Hirschmeier, C. Chen, J. Avila, M. C. Asensio, A. A. Zakharov, T. O. Wehling, A. I. Lichtenstein, M. I. Katsnelson, and U. Starke, Introducing strong correlation effects into graphene by gadolinium intercalation, Phys. Rev. B **100**, 121407(R) (2019).

[10] C. Riedl, C. Coletti, T. Iwasaki, A. A. Zakharov, and U. Starke, Quasi-Free-Standing Epitaxial Graphene on SiC Obtained by Hydrogen Intercalation, Phys. Rev. Lett. **103**, 246804 (2009).

[11] S. Watcharinyanon, L. I. Johansson, C. Xia, J. Ingo Flege, A. Meyer, J. Falta, and C. Virojanadara, Ytterbium intercalation of epitaxial graphene grown on Si-face SiC, Graphene **2**, 66 (2013).

[12] S. Sung, S. Kim, P. Lee, J. Kim, M. Ryu, H. Park, K. Kim, B. Il Min, and J. Chung, Observation of variable hybridized-band gaps in Eu-intercalated graphene, Nanotechnology **28**, 205201 (2017).

[13] F. Calleja, H. Ochoa, M. Garnica, S. Barja, J. J. Navarro, A. Black, M. M. Otrokov, E. V. Chulkov, A. Arnau, A. L. Vázquez de Parga, F. Guinea, and R. Miranda, Spatial variation of a giant spin–orbit effect induces electron confinement in graphene on Pb islands, Nat. Phys. **11**, 43 (2015).

[14] A. M. Shikin, A. G. Rybkin, D. Marchenko, A. A. Rybkina, M. R. Scholz, O. Rader, and A. Varykhalov, Induced spin-orbit splitting in graphene: The role of atomic number of the intercalated metal and π-d hybridization, New J. Phys. **15**, 13016 (2013).

[15] S. D. Bader, Colloquium: Opportunities in nanomagnetism, Rev. Mod. Phys. **78**, 1 (2006).

[16] K. Kanetani, K. Sugawara, T. Sato, R. Shimizu, K. Iwaya, T. Hitosugi, and T. Takahashi, Ca intercalated bilayer graphene as a thinnest limit of superconducting C6Ca, Proc. Natl. Acad. Sci. USA **109**, 19610 (2012).

[17] S. Ichinokura, K. Sugawara, A. Takayama, T. Takahashi, and S. Hasegawa, Superconducting calcium-intercalated bilayer graphene, ACS Nano **10**, 2761 (2016).

[18] Y. Endo, Y. Fukaya, I. Mochizuki, A. Takayama, T. Hyodo, and S. Hasegawa, Structure of superconducting Ca-intercalated bilayer graphene/SiC studied using total-reflection high-energy positron diffraction, Carbon N.Y. **157**, 857 (2020).

[19] J. C. Kotsakidis, A. Grubišić-Čabo, Y. Yin, A. Tadich, R. L. Myers-Ward, M. DeJarld, S. P. Pavunny, M. Currie, K. M. Daniels, C. Liu, M. T. Edmonds, N. V. Medhekar, D. K. Gaskill, A. L. Vázquez de Parga, and M. S. Fuhrer, Freestanding n-doped graphene via intercalation of calcium and magnesium into the buffer layer–SiC(0001) interface, Chem. Mater. **32**, 6464 (2020).

[20] Y. Zhang, H. Zhang, Y. Cai, J. Song, D. Qiao, Q. Chen, F. Hu, P. Wang, K. Huang, and P. He, Calcium intercalation underneath N-layer graphene on 6H-SiC(0001), Chem. Phys. Lett. **703**, 33 (2018).

[21] H. Toyama, R. Akiyama, S. Ichinokura, M. Hashizume, T. Iimori, Y. Endo, R. Hobara, T. Matsui, K. Horii, S. Sato, T. Hirahara, F. Komori, and S. Hasegawa, Two-dimensional superconductivity of Ca-intercalated graphene on SiC: Vital role of the interface between monolayer graphene and the substrate, ACS Nano **16**, 3582 (2022).

[22] J. D. Emery, B. Detlefs, H. J. Karmel, L. O. Nyakiti, D. K. Gaskill, M. C. Hersam, J. Zegenhagen, and M. J. Bedzyk, Chemically Resolved Interface Structure of Epitaxial Graphene on SiC(0001), Phys. Rev. Lett. **111**, 215501 (2013).

[23] M. Conrad, J. Rault, Y. Utsumi, Y. Garreau, A. Vlad, A. Coati, J.-P. Rueff, P. F. Miceli, and E. H. Conrad, Structure and evolution of semiconducting buffer graphene grown on SiC(0001), Phys. Rev. B **96**, 195304 (2017).

[24] M. A. Hove, W. H. Weinberg, and C. M. Chan, in *Low-Energy Electron Diffraction Experiment, Theory and Surface Structure Determination*, Springer Series in Surface Sciences (SSSUR, Vol. 6) (Springer, Berlin, 1986).

[25] M. Hupalo, E. H. Conrad, and M. C. Tringides, Growth mechanism for epitaxial graphene on vicinal 6H-SiC(0001) surfaces: A scanning tunneling microscopy study, Phys. Rev. B **80**, 041401(R) (2009).

[26] C. Riedl, U. Starke, J. Bernhardt, M. Franke, and K. Heinz, Structural properties of the graphene-SiC(0001) interface as a key for the preparation of homogeneous large-terrace graphene surfaces, Phys. Rev. B **76**, 245406 (2007).

[27] S. Chen, M. Horn von Hoegen, P. A. Thiel, and M. C. Tringides, Diffraction paradox: An unusually broad diffraction background marks high quality graphene, Phys. Rev. B **100**, 155307 (2019).

[28] S. Stepanovsky, M. Yakes, V. Yeh, M. Hupalo, and M. C. Tringides, The dense α-$\sqrt{3}\times\sqrt{3}$Pb/Si(111) phase: A comprehensive STM and SPA-LEED study of ordering, phase transitions and interactions, Surf. Sci. **600**, 1417 (2006).

[29] Y. Han, J. W. Evans, and M. C. Tringides, Dy adsorption on and intercalation under graphene on 6*H*-SiC(0001) surface from first-principles calculations, Phys. Rev. Mater. **5**, 074004 (2021).

[30] See Supplemental Material at http://link.aps.org/supplemental/10.1103/PhysRevB.107.045408 for Figs. S1–S4, typical fits of the diffraction spot profiles; Fig. S5 shows pristine graphene morphology and after Dy deposition at RT.

[31] K. V. Emtsev, A. A. Zakharov, C. Coletti, S. Forti, and U. Starke, Ambipolar doping in quasifree epitaxial graphene on SiC(0001) controlled by Ge intercalation, Phys. Rev. B **84**, 125423 (2011).

[32] W. Li, L. Huang, M. C. Tringides, J. W. Evans, and Y. Han, Thermodynamic preference for atom adsorption on versus intercalation into multilayer graphene, J. Phys. Chem. Lett. **11**, 9725 (2020).

[33] M. Narayanan Nair, M. Cranney, T. Jiang, S. Hajjar-Garreau, D. Aubel, F. Vonau, A. Florentin, E. Denys, M.-L. Bocquet, and L. Simon, Noble-metal intercalation process leading to a protected adatom in a graphene hollow site, Phys. Rev. B **94**, 075427 (2016).

[34] I. Gierz, T. Suzuki, R. T. Weitz, D. S. Lee, B. Krauss, C. Riedl, U. Starke, H. Höchst, J. H. Smet, C. R. Ast, and K. Kern, Electronic decoupling of an epitaxial graphene monolayer by gold intercalation, Phys. Rev. B **81**, 235408 (2010).

[35] S. Forti, S. Link, A. Stöhr, Y. Niu, A. A. Zakharov, C. Coletti, and U. Starke, Semiconductor to metal transition in two-dimensional gold and its van der Waals heterostack with graphene, Nat. Commun. **11**, 2236 (2020).

[36] L. H. de Lima, R. Landers, and A. de Siervo, Patterning quasi-periodic Co 2D-Clusters underneath graphene on SiC(0001), Chem. Mater. **26**, 4172 (2014).

[37] G. S. Grebenyuk, E. Y. Lobanova, D. A. Smirnov, I. A. Eliseev, A. V. Zubov, A. N. Smirnov, S. P. Lebedev, V. Y. Davydov, A. A. Lebedev, and I. I. Pronin, Cobalt intercalation of graphene on silicon carbide, Phys. Solid State **61**, 1316 (2019).

[38] R. Hönig, P. Roese, K. Shamout, T. Ohkochi, U. Berges, and C. Westphal, Structural, chemical, and magnetic properties of cobalt intercalated graphene on silicon carbide, Nanotechnology **30**, 025702 (2019).

[39] L. Daukiya, M. N. Nair, S. Hajjar-Garreau, F. Vonau, D. Aubel, J. L. Bubendorff, M. Cranney, E. Denys, A. Florentin, G. Reiter, and L. Simon, Highly n-doped graphene generated through intercalated terbium atoms, Phys. Rev. B **97**, 035309 (2018).

[40] J. Kleeman, K. Sugawara, T. Sato, and T. Takahashi, Direct evidence for a metallic interlayer band in Rb-intercalated bilayer graphene, Phys. Rev. B **87**, 195401 (2013).

[41] M. Kolmer, B. Schrunk, M. Hupalo, J. Hall, S. Chen, J. Zhang, C.-Z. Wang, A. Kaminski, and M. C. Tringides, Highly asymmetric graphene layer doping and band structure manipulation in rare earth–graphene heterostructure by targeted bonding of the intercalated gadolinium, J. Phys. Chem. C **126**, 6863 (2022).

[42] K. Su Kim, A. L. Walter, L. Moreschini, T. Seyller, K. Horn, E. Rotenberg, and A. Bostwick, Coexisting massive and massless Dirac fermions in symmetry-broken bilayer graphene, Nat. Mater. **12**, 887 (2013).

[43] K. Omambac, M. Kriegel, C. Brand, B. Finke, L. Kremeyer, H. Hattab, D. Janoschka, P. Dreher, F.-J. Meyer zu Heringdorf, D. Momeni Pakdehi, K. Pierz, H. W. Schumacher, M. Petrović, A. van Houselt, B. Poelsema, M. C. Tringides, and M. Horn-von Hoegen, Non-conventional bell-shaped diffuse scattering in low-energy electron diffraction from high-quality epitaxial 2D-materials, Appl. Phys. Lett. **118**, 241902 (2021).

[44] T. Ohta, A. Bostwick, J. L. McChesney, T. Seyller, K. Horn, and E. Rotenberg, Interlayer Interaction and Electronic Screening in Multilayer Graphene Investigated with Angle-Resolved Photoemission Spectroscopy, Phys. Rev. Lett. **98**, 206802 (2007).

[45] T. A. de Jong, E. E. Krasovskii, C. Ott, R. M. Tromp, S. J. van der Molen, and J. Jobst, Intrinsic stacking domains in graphene on silicon carbide: A pathway for intercalation, Phys. Rev. Mater. **2**, 104005 (2018).

[46] T. Hirahara, S. V. Eremeev, T. Shirasawa, Y. Okuyama, T. Kubo, R. Nakanishi, R. Akiyama, A. Takayama, T. Hajiri, S.-I. Ideta, M. Matsunami, K. Sumida, K. Miyamoto, Y. Takagi, K. Tanaka, T. Okuda, T. Yokoyama, S.-I. Kimura, S. Hasegawa, and E. V. Chulkov, Large-gap magnetic topological heterostructure formed by subsurface incorporation of a ferromagnetic layer, Nano Lett. **17**, 3493 (2017).

[47] S. Schumacher, T. O. Wehling, P. Lazić, S. Runte, D. F. Förster, C. Busse, M. Petrović, M. Kralj, S. Blügel, N. Atodiresei, V. Caciuc, and T. Michely, The backside of graphene: Manipulating adsorption by intercalation, Nano Lett. **13**, 5013 (2013).

[48] X. Liu, C.-Z. Wang, M. Hupalo, H.-Q. Lin, K.-M. Ho, P. A. Thiel, and M. C. Tringides, Metal intercalation-induced selective adatom mass transport on graphene, Nano Res. **9**, 1434 (2016).

[49] T. Ohta, A. Bostwick, T. Seyller, K. Horn, and E. Rotenberg, Controlling the electronic structure of bilayer graphene, Science **313**, 951 (2006).